SCIENCE CHINA
Earth Sciences

• RESEARCH PAPER •

June 2010 Vol.53 No.6: 892–900
doi: 10.1007/s11430-010-0078-z

An englacial image and water pathways of the Fourcade glacier on King George Island, Antarctic Peninsula, inferred from ground-penetrating radar

LEE Joohan[1*], KIM Ki Young[2], HONG Jong Kuk[1] & JIN Young Keun[1]

[1] *Korea Polar Research Institute, Songdo Techno Park, 7-50, Songdo-dong, Yeonsu-gu, Incheon 406-840, Korea;*
[2] *Department of Geophysics, Kangwon National University, Chunchon, 200-701, Korea*

Received May 21, 2009; accepted April 13, 2010; published online May 12, 2010

The distribution of small fractures and water content of the Fourcade glacier on King George Island, Antarctica, was investigated in November 2006 and December 2007 by two ground-based (470- and 490-m-long profiles) and one helicopter-borne (470-m-long profile) ground-penetrating radar (GPR) surveys using 50-, 100-, and 500-MHz antennas. Radar images in the pre-migrated GPR sections are characterized by a smooth ice surface and irregular bed topography, numerous diffraction hyperbolas in the ice and at the glacier bed, strong scattering noise, and near-surface folded layers. Scattering noise above a mound in the center of the profiles is associated with an area of dense fractures extending down from the ice surface that has relatively low reflection strength. Near the northeast ends of the profiles where few englacial fractures occur, scattering noise may result from the presence of warmer ice. A water-filled conduit and an air-filled cavity are interpreted as the source of two distinct hyperbolas in sub-glacial valleys based on the polarity of the reflections. Through migration velocity analysis on 106 hyperbolas, radar velocities were obtained for the 100-MHz ground-based profile. Using the velocities and Paren's mixture formula, we calculated the water content of the ice to have been in the range of 0.00–0.09. High water content occurs near the glacier margin, in sub-glacial valleys, and in zones of scattering noise.

GPR, water content, Fourcade glacier, scattering noise, migration velocity analysis, fractures

Citation: Lee J, Kim K Y, Hong J K, et al. An englacial image and water pathways of the Fourcade glacier on King George Island, Antarctic Peninsula, inferred from ground-penetrating radar. Sci China Earth Sci, 2010, 53: 892–900, doi: 10.1007/s11430-010-0078-z

1 Introduction

Many studies of glacier hydrology have been conducted using ground-penetrating radar (GPR), which is based on the excellent penetration of radio waves through ice. Emitted electromagnetic (EM) waves penetrate snow and ice bodies and are reflected at internal boundaries between media with different dielectric constants, such as annual snow and firn layers, as well as at the glacier bed.

The common midpoint (CMP) method is widely applied [1] to the study of both englacial and subglacial environments [1–3], but the common-offset method, which is less time consuming, can also be used. In the common-offset method, migration velocity analysis (MVA) is used to obtain radar velocities of ice. Bradford and Harper [2] used the MVA method coupled with dielectric modeling to determine the englacial water content of a temperate glacier. Concepts of basal reflection strength (BRS) and bed reflection power (BRP) also facilitate delineation of discrete englacial and subglacial water bodies [4, 5].

Radar reflection data are commonly contaminated by

*Corresponding author (email: joohan@kopri.re.kr)

noise, some of which includes useful information. For example, Rayleigh scattering, which is generated from particles that are smaller than the wavelength of the radar signal, is generally regarded as noise [6]. In this study, three GPR cross-sections near the western margin of the Fourcade glacier on King George Island (KGI), Antarctica, (Figure 1) were used to generate englacial radar images and interpret the spatial variation of englacial water content. Such interpretations are based on the assumption that the radar velocity of ice is affected most strongly by its water content [1–3, 7, 8]. Diffraction velocity and the polarity of hyperbolas derived from the ground-based GPR profiles and reflection strength (RS) of airborne radar data are used to determine characteristics related to possible englacial water storage.

2 Data acquisition and basic processing

In the austral summers of 2006–2007 and 2007–2008, shallow geophysical surveys were conducted roughly perpendicular to the maximum slope of the glacier surface in the ablation zone of the western Fourcade glacier (Figure 1). In November 2006, ground-based GPR and 24-channel high-resolution seismic data were recorded along the 470-m-long Profile G1, and more than 298 km of helicopter-borne radar data were obtained near the ground-based profile. Additional ground-based GPR data were acquired in December 2007 along the 490-m-long Profile G2, which crosses Profile G1 at an angle of 22°. This study is based on the high-frequency GPR data from Profile G1, the lower-frequency data from Profile G2, and airborne radar data from Profile H1.

The geophysical instrument used during the radar survey was a RAMAC/GPR system (Måla GeoScience). Along Profile G1, radar antennas with center frequencies of 50, 100, and 500 MHz were used to identify targets at various depths. This study is based on the higher-resolution radar data from Profile G1, which were collected with shielded 100- and 500-MHz antennae with transmitter–receiver distances of 0.50 m and 0.18 m, respectively. In Profile G2, an unshielded antenna with a center frequency of 50 MHz and transmitter-receiver distance of 3.50 m was towed behind a snowmobile. For each trace of the 50-, 100-, and 500-MHz data, 504, 939, and 1024 samples were digitized using time windows of 2031, 1171, and 209 ns, respectively. The average trace intervals were 0.079, 0.061, and 0.097 m after 16-, 4-, and 4-fold vertical stacking of the 50-, 100-, and 500-MHz data, respectively.

Helicopter-borne radar data were acquired along Profile H1, almost parallel to Profile G1, using the same shielded antenna with a 100-MHz center frequency. The antenna was mounted between the skids of the helicopter, with the transmitter and the receiver set in the fore and aft. The helicopter flew above the glacier surface at an average height of 12.73 m and an average speed of 18.8 m/s. The flight altitude was calculated based on the first break of radar signals. Average trace spacing of the airborne data was approximately 1.2 m. During the airborne GPR surveys, positional data were collected using a portable GPS. GPS signals were also recorded on the ground for differential GPS post-processing.

After the location and elevation for each trace were determined, trace editing and removal of DC components were applied. Zero-phase band-pass filters with bandwidths of 25–80, 60–150, and 250–730 MHz were then applied to attenuate both high- and low-frequency noise after geometric spreading corrections by programmed gain control. Ringing background noise was removed by subtracting the mean trace from each trace. Normal moveout (NMO) corrections were then applied using the 0.16-m/ns radar velocity of ice for constant offsets of 3.50, 0.50, and 0.18 m for 50-, 100-, and 500-MHz data, respectively. Single-channel recording prevented the application of NMO velocity analysis, and instead, medium velocities were determined using

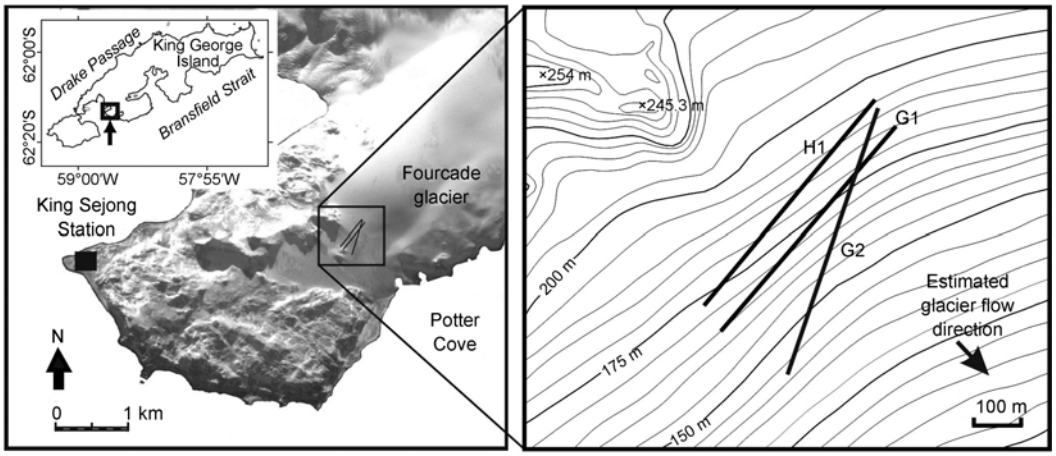

Figure 1 Map of the western Fourcade glacier with locations of GPR profiles G1, G2, and H1, all roughly perpendicular to the maximum slope of the ice surface.

the *f-k* migration velocity analysis (MVA) method based on the Stolt algorithm [9]. In this method, the optimal migration velocity collapses a diffraction hyperbola to a point, and erroneously lower and higher velocities result in under- and over-migration with the appearance of "frowns" and "smiles", respectively. In Profile G1, 106 hyperbolas were analyzed using the MVA method with a 0.001-m/ns interval in the migration velocity range of 0.080–0.200 m/ns. The hyperbolas that are relatively evenly distributed at the ice-bed interface are associated with irregular sub-glacial topography and inhomogeneities in weathered volcanic rocks or moraine deposits (Figure 2). To minimize measurement errors and avoid artifacts, diffraction curves in the noisy zone (f4 in Figure 2) were not analyzed.

3 Major englacial features

Five distinctive features are present in the pre-migrated GPR sections in Profiles G1 and G2 (Figures 2–4): reflections from the smooth air-ice interface, reflections from an irregular glacier bed, distinct hyperbolas generated by diffractors, strong scattering noise in which distinct hyperbolas cannot be interpreted, and reflections from near-surface englacial layering or foliation. The helicopter-borne profile H1 (Figure 5) also shows similar englacial and subglacial features to those depicted along Profiles G1 and G2, although the signal-to-noise ratios were much lower than those of the ground-based data.

The boundaries at the ice surface and the glacier bed are distinct due to relatively large differences in dielectric constant between the ice and the air and rock layers. The smooth ice surface is higher at the northeast ends of Profiles G1 and G2 than at their southwest ends by 30 m and 45 m, respectively. Assuming a radar velocity in ice of 0.16 m/ns, the maximum thickness of ice in the two GPR profiles is about 66m near the northeast end of Profile G2. The thalweg of a subglacial valley is interpreted at profile distances of 189 m in Profile G1 (Figure 2) and 190 m in Profile G2 (Figure 4), which are separated by 68 m. This southwest-trending valley narrows toward the glacier terminus (Figure 1).

The polarity of radar signals reflected at the ice-basement boundary in the radar section (Figure 2(b)) is (+-+), which

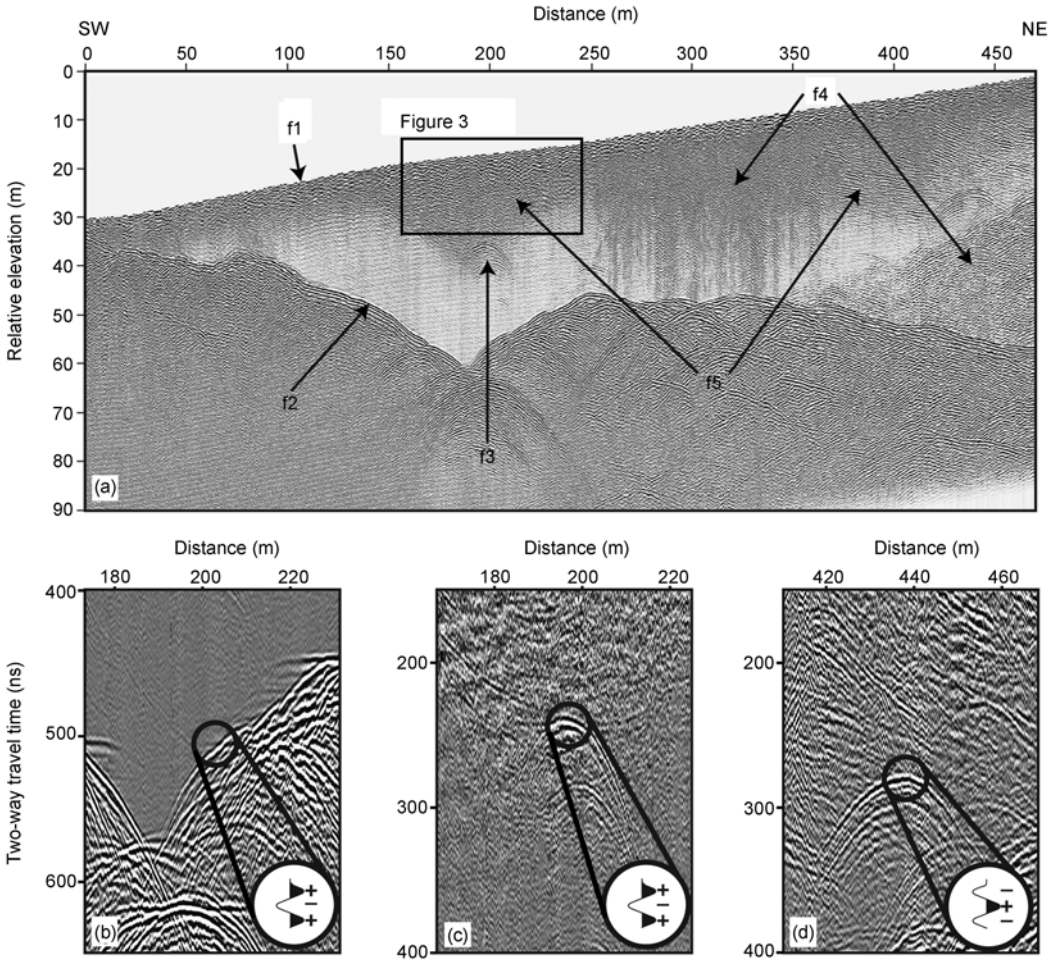

Figure 2 A 100-MHz pre-migrated GPR section along Profile G1 and polarity images of the diffraction hyperbolas. f1, the smooth ice surface; f2, irregular glacier bed; f3, hyperbola generated by diffractors; f4, scattering noise; f5, near-surface englacial layering or foliation.

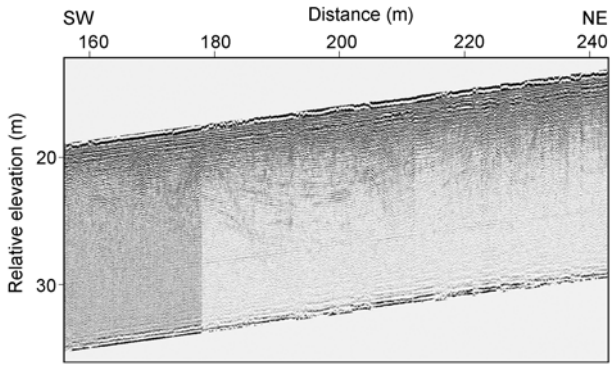

Figure 3 A high-frequency radar section, obtained using a 500-MHz antenna along Profile G1, showing detailed structures of the bent layers.

is regarded as a reversed polarity. A hyperbola at a distance of 196 m in Profile G1 (Figure 2(c)) has a reversed (+-+) polarity, whereas one at 437 m (Figure 2(d)) has a normal (-+-) polarity. This indicates that these two hyperbolas were caused by diffractors with smaller and greater dielectric constants, respectively, than that of the ice. Similar hyperbolic features are present at distances of 187 and 330 m in Profile G2 (Figure 4).

Bent layers are present outside the scattering zone (Figures 2–4). The layers are continuous and subparallel to the glacier bed, and terminate at the glacier surface as toplap. The bent layers have an average individual layer thickness of 0.17 m and apparently lap out near the air-ice boundary at distances of 160–240 m (Figure 3). Apparent dips of the toplap relationships near 160 and 240 m are 11.93°NE and 10.87°SW, respectively.

4 Water content of the ice from ground-based GPR data

The dielectric constant of ice is known to be sensitive to water content. Although empirical formulas relating meas-

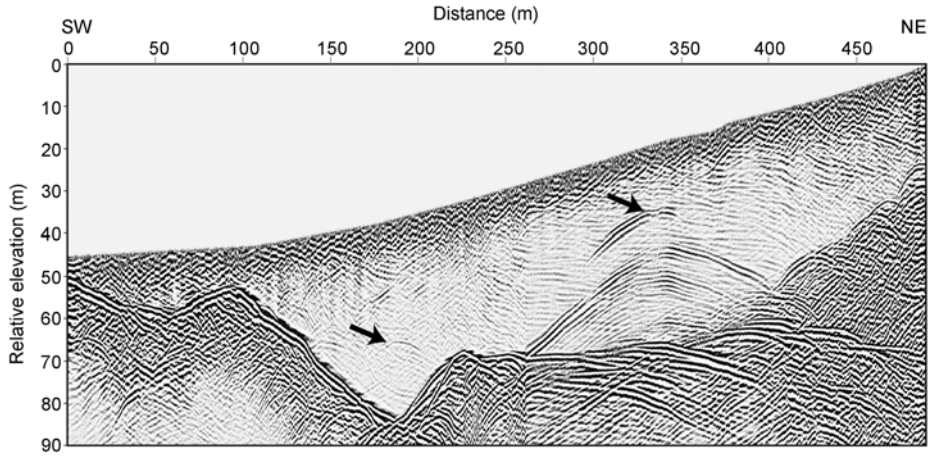

Figure 4 A 50-MHz pre-migrated GPR section along Profile G2. The black arrows indicate hyperbolas. Profile G2 crosses Profile G1 at a distance of 350 m at an angle of 22°. A valley centered at a profile distance of 190 m is narrower than that in Profile G1 (Figure 2).

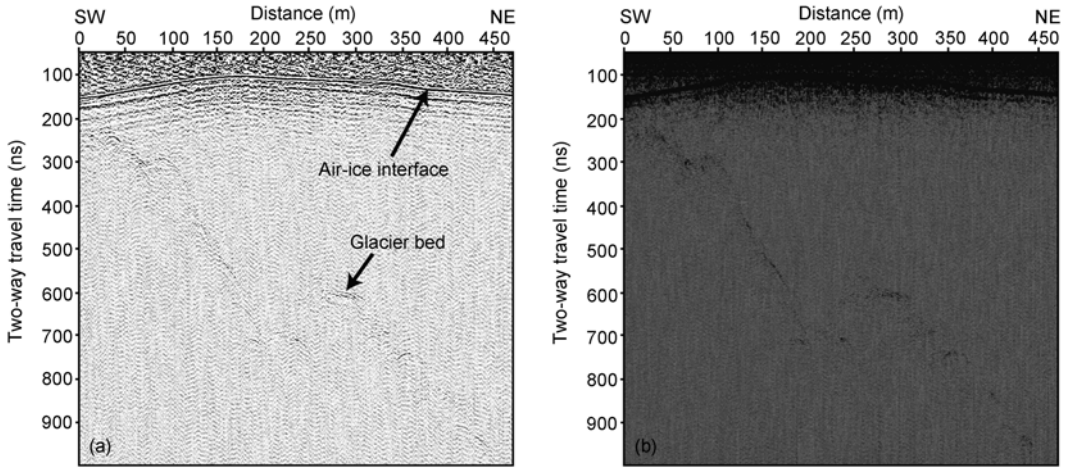

Figure 5 A helicopter-borne GPR section along Profile H1 (a) and its instantaneous amplitude (b). The signal-to-noise ratio is pronounced compared to that of the ground-based GPR (Figure 2). The highest horizontal reflector in the time range of 100–150 ns denotes the air-ice interface. Instantaneous amplitude shows spatial variation of RS.

ured dielectric constant to the water content of materials are widely used for soils and rocks, Looyenga's [10] and Paren's [11] empirical relationships are known to be better when the dielectric constants are close to the value of ice [1, 12]. Paren's mixture formula was used to calculate the water content of the ice from radar velocities:

$$\theta_{\mathrm{w}} = \frac{3}{\varepsilon_{\mathrm{w}}}\left(\frac{c^2}{v^2} - \varepsilon_i\right), \tag{1}$$

where θ_{w} is water content by volume, ε_{w} and ε_i are relative permittivities of water (80) and ice (3.2), respectively, c is the speed of light in a vacuum, and v is the measured radar velocity.

The migration velocities obtained using the MVA method were interpolated using the kriging technique for 35000 grid points with horizontal spacing of 1.3 m and vertical spacing of 0.8 m. After the velocity functions were smoothed using a two-dimensional polynomial function, interval velocities were computed using the Dix equation [13]. Most of the computed values for water content in Profile G1 are in the range of 0.000–0.090 (Figure 6). High water contents are indicated near the western edge of the profile (distance 30 m), in sub-glacial valleys centered on distances of 160 and 210 m, and in the scattering noise zones between distances 270 and 370 m and near the northeast end. The computed water content is close to zero near the ice surface at distances of 140–170 m and northeast of 380 m. Another area of low water content is near the bed over the subglacial high.

5 Reflection strength from the helicopter-borne GPR data

In GPR data recorded from the air, the reflection strength (RS) of the radar return from the air-ice interface can indicate the electromagnetic properties of that surface. The RS is controlled by the permittivities of air and ice and can be used to infer the wetness of the ice surface [4, 5, 14, 15]. The RS varies with the altitude, direction, and dip of the antenna. The antenna was fixed between the helicopter skids during the GPR survey, and so its orientation relative to the profiles gathered can be regarded as constant. Assuming that the helicopter's attitude relative to horizontal did not change during the flight, the only factor that must be compensated for in calculating the wetness of the ice surface is the altitude. Figure 7 shows the effect of antenna altitude on RS, where the antenna altitude and the RS are inversely related.

The geometrical effect of source altitude was calculated using two-dimensional finite-difference time-domain (FDTD) modeling based on Maxwell's equations [16]. The normalized RS at the air–ice interface was calculated for source altitudes in the range of 2–50 m (Figure 7(c)). A best-fit curve was derived as a power of altitude:

$$R_{\mathrm{ai}} = 1.211 \cdot h^{-0.4282}, \tag{2}$$

where R_{ai} is the relative RS at the air-ice interface, and h is the altitude of the source. The RS decreases rapidly as source altitude increases. The geometrical correction factors were then calculated for all source altitudes along Profile H1.

The footprint over which an RS is estimated may be represented by the first Fresnel zone [17], which is approximately 8.74 m at an average flight altitude of 12.73 m. The average trace spacing of 1.2 m along Profile H1 is much smaller than the first Fresnel zone. Although total RS loss at the air-ice boundary depends on surface roughness [15], the scattering loss from the ice–air interface was not considered in further analyses because the ice surface in the study area was relatively flat based on the Rayleigh criterion (~1/8 of the wavelength; [18]). Therefore, the relative RS at the air-ice boundary indicates the relative wetness of the glacier surface. The relative RS is high for distances of 120–260 m along Profile H1 (Figure 8(a)). This part of the profile coin-

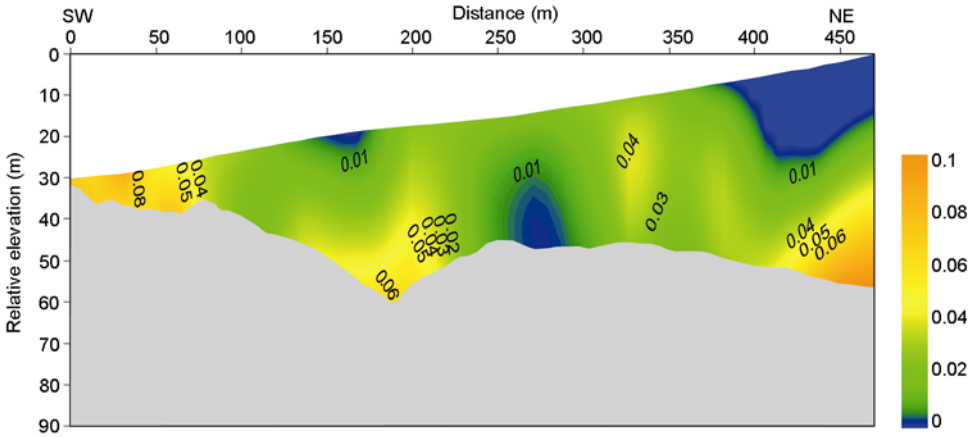

Figure 6 Estimated water content using Paren's mixture formula with the velocity calculated from MVA. The estimation error associated with the MVA method is less than 0.002 m/ns.

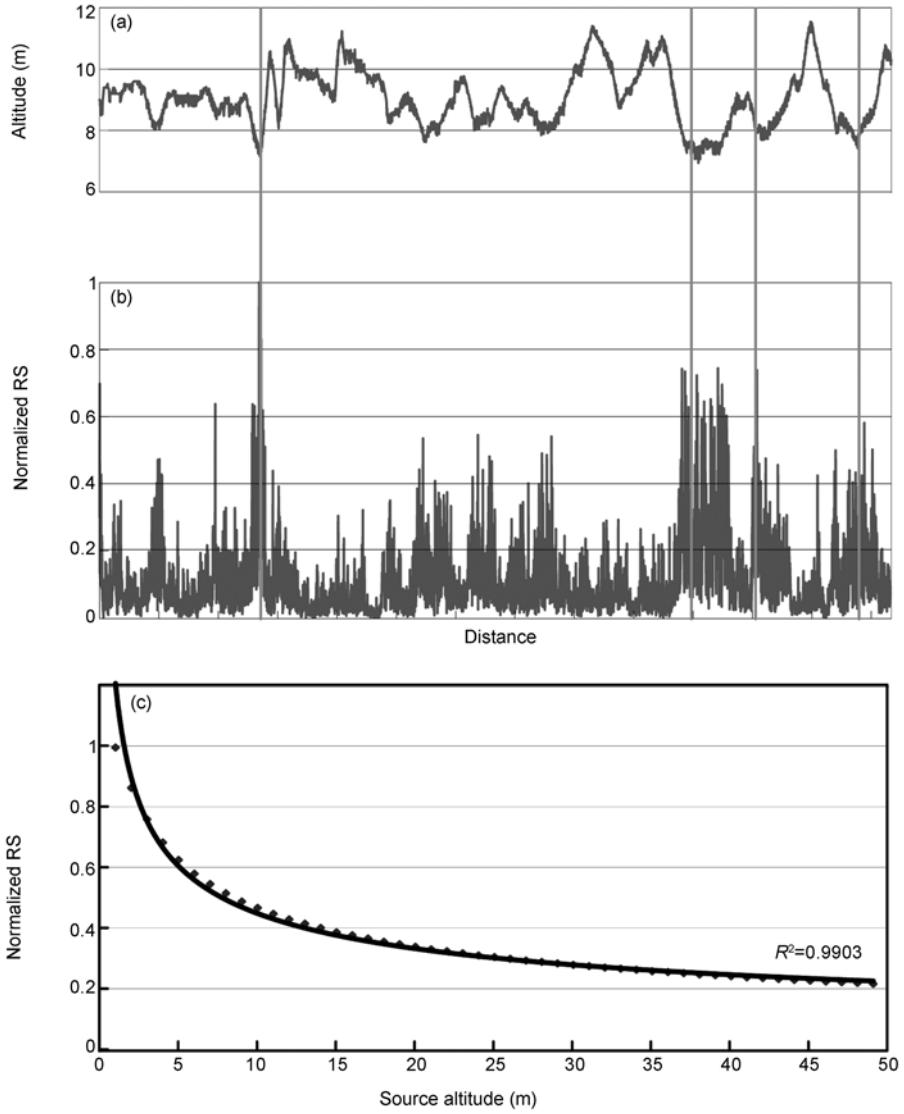

Figure 7 The effect of antenna altitude on RS ((a), (b)) and geometrical correction function with source altitudes in the range of 2–50 m, calculated at the air-ice interface with the FDTD method (c). The RSs are inversely related to antenna altitude.

cides with a dark area in the aerial photograph (black arrows in Figure 8(b)). The relative RS is below average where scattering noise masks the englacial structure in the 260–360 m range of Profile G1. This indicates that the scattering noise may not be related to surface water origin [19] but instead to dense fractures in the ice body [20, 21].

6 Discussion

6.1 Scattering zone

An approximately 100-m-wide region of strong noise is present above the mound structure centered at a profile distance of 247 m (Figure 2). This scattering zone is characterized by high-angle semi-linear structures extending from the glacier surface to its base. In this strong-noise region, a relatively high water content of 0.03–0.043 was calculated from the radar velocities using eq. (1) 1 (Figure 6). Murray et al. [1] showed that a radar velocity of 0.149 m/ns in ice corresponded to a water content of 0.03–0.041 and interpreted this to be the glacier's internal piezometric water level. The possibility that the scattering noise was generated by ringing of radar waves due to water storage on the surface [19] can be dismissed based on the absence of water on the surface in the aerial photograph that was taken at the same time (Figure 8(b)). The relative RS at the air-ice boundary provided by the airborne radar data (Figure 8(a)) reflects the relative water content of the glacier surface. The average RS of 0.619 in the scattering zone is even lower than the average value for the entire profile range (0.666), which indicates that the scattering noise was probably not generated by superficial water storage.

Water- and air-filled fractures in the glacier affect electromagnetic and seismic wave velocities because both ve-

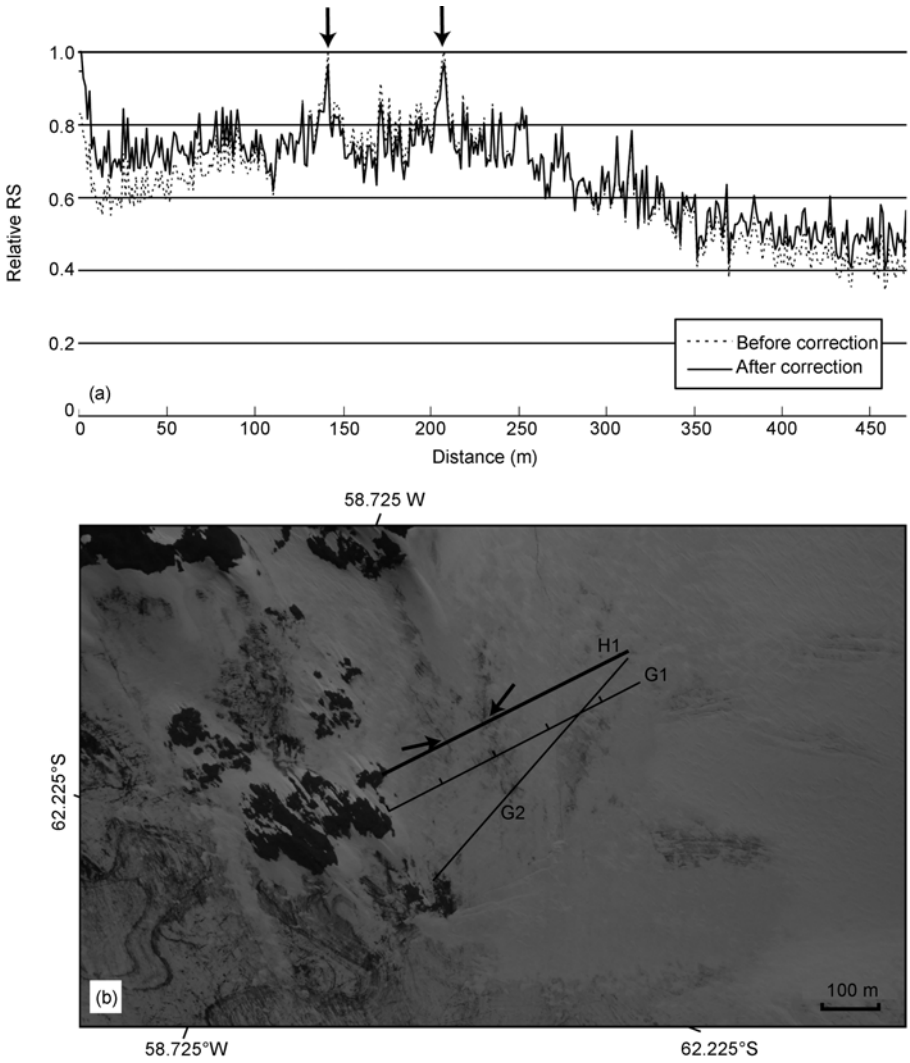

Figure 8 Relative RS calculated from helicopter-based GPR data (a) and aerial photographs of the survey area (b). Black arrows indicate two peak points of relative RS. The two points of relative RS in (a) match well with discolored ice where linear structures are well developed.

locities depend primarily on the bulk properties of the media. The seismic P-wave velocities in Profile G1, determined by the refraction tomography method, vary between 3000 and 3700 m/s in the ice body (Figure 9) [21]. The average P-wave velocity in the scattering zone is approximately 3320 m/s, which is well below the near-surface ice velocity of 3525 ± 198 m/s in the ablation zone of Johnson's glacier [22]. Such low seismic velocities in the strong-noise zone may indicate that the scattering noise is due to dense fractures. Given that the GPR data were recorded during the melting season and frequent summer rains occurred, it can be assumed that englacial fractures were partly or fully water filled.

Similar noise patterns have been noticed and interpreted by many, including Fountain et al. [20] and Irvine-Fynn et al. [19]. Fountain et al. [20] drilled 48 bore holes in the Storglaciären glacier and encountered fractures 0.3 to 20 cm wide. They concluded that fractures are the main pathways by which surface water is delivered deep into the glacier.

Another zone of strong scattering noise appears near the northeast end of the profile, where englacial fractures are apparently scarce. In contrast to the noise above the mound, the scattering noise in this area may be not directly related to fractures. Relatively low radar velocities and the scarcity of fractures suggest that the scattering noise in this region was probably caused by warmer ice.

6.2 Folded layers and hyperbolas

Folded layers were imaged outside the scattering zone. Folded structures may arise from lateral compression of original ice layers in areas where ice flow is constricted by narrowing of the valley [23]. Lap-out features of the layers at the glacier surface were imaged in the aerial photograph taken during the same campaign (Figure 8(b)). They are partially discolored and show a sub-linear pattern that is approximately perpendicular to the maximum slope of the glacier surface. The location of high RS in the radar profile

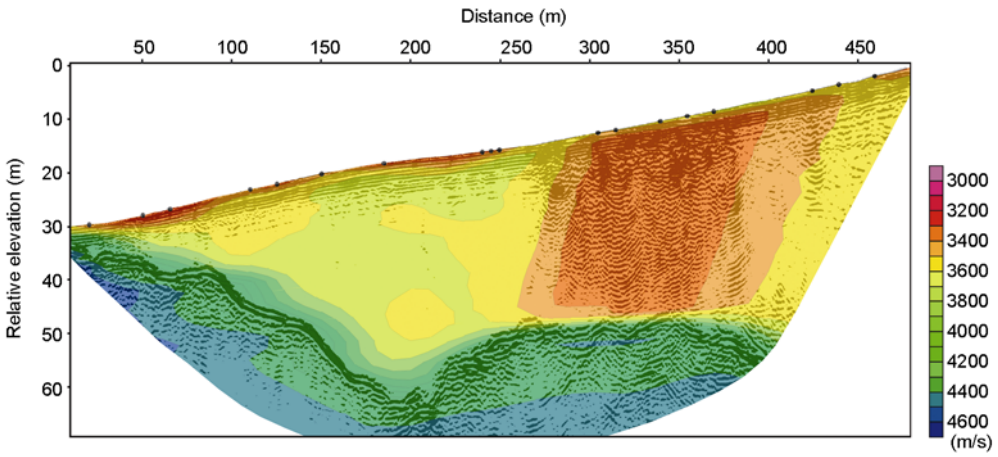

Figure 9 P-wave velocity tomogram for the seismic profile indicating a distinctive low-velocity region associated with the scattering zone of Figure 2 (modified from Kim et al. [21]).

H1 (Figure 8(a)) coincides with the surface location where the folded layers terminate. The high RS seems to be related to high water content in water-saturated bubbly or impurity-rich ice layers intercalated with solid ice layers.

The diffraction hyperbola in the folded layers at 196-m distance (Figure 2(c)) has a reversed polarity. This indicates that the diffractor is probably a water-filled cavity [24]. This is consistent with extremely high water content of 0.035–0.050 at the relative elevation range of 36–46 m (Figure 6) and with low P-wave velocities (Figure 9) in the vicinity of the apex of diffraction. Profile G2 also shows a similar hyperbolic feature on the folded layer at a distance of 187 m (Figure 4). Considering both the relatively short distance (60 m) between the diffractors in profiles G1 and G2 and the orientation of the two apexes roughly parallel to the maximum slope of the surface, we think that the two cavities identified in the GPR sections may connect to form an englacial channel.

The hyperbola at 437-m distance and 21.8-m depth in profile G1 (Figure 2(d)) has a normal polarity (-+-), which may indicate that at least the upper part of the void space was filled with air. The calculated value of water content is very close to zero here. A high water content of 0.04–0.09 approximately 10 m below the hyperbola indicates the presence of warm ice.

7 Conclusions

Both subglacial and englacial radar images and the calculated water contents of the ice in the ablation zone of the Fourcade glacier were investigated using ground-based and helicopter-borne GPR. The most distinctive features are the smooth ice surface and irregular glacier bed, hyperbolas generated by diffractors, scattering noise in a highly fractured zone and in areas of warm ice, and near-surface curved layers or foliations. Possible water pathways are identified by their strong diffraction patterns. Based on the polarity of the diffraction hyperbolas, a hyperbola in the subglacial valley in the middle of the profiles is interpreted as a water-filled conduit, whereas a second hyperbola near the northeast end of the profiles is believed to be at least partly air-filled.

The water content calculated using radar velocities is in the range of 0.00–0.09 for Profile G1. High water content is indicated near the southwest end of the profile, in the sub-glacial valleys, in the densely fractured zone of scattering noise, and in the warmer ice near the northeast end. The relative RS is high above the sub-glacial valley, where a dark area appears in the aerial photograph. Low RS in the scattering noise zone indicates that the scattering noise may not be due to surface water but to a high density of fractures in the ice.

We thank Dr. Moon Young Choe, chief of the 19th over-wintering team of King Sejong Station, and his team-members who helped us during acquisition of the radar data. We also thank two anonymous referees who gave thoughtful and helpful comments that improved the manuscript. Finally we appreciate Dr. R. M. Rene at Rene Geophysics for his helpful discussions and suggestions during the progress of this work. This work was supported by Korea Polar Research Institute (KOPRI) (Grant Nos. PE10020, PM09030) and the Korea Science and Engineering Foundation (KOSEF) of the Ministry of Science and Technology (MOST) (Grant No. R01-2007-000-20194-0).

1 Murray T, Stuart G W, Fry M, et al. Englacial water distribution in a temperate glacier from surface and borehole radar velocity analysis. J Glaciol, 2000, 4: 389–398
2 Bradford J H, Harper J T. Wave field migration as a tool for estimating spatially continuous radar velocity and water content in glaciers. Geophys Res Lett, 2005, 32: L08502, doi: 08510.01029/02004GL021770
3 Murray T, Booth A, Rippin D M. Water-content of glacier-ice: Limitations on estimates from velocity analysis of surface ground-penetrating radar surveys. J Environ Eng Geophys, 2007, 12: 87–99
4 Bingham R G, Siegert M J. Radio-echo sounding over polar ice masses. J Environ Eng Geophys, 2007, 12: 47–62

5 Woodward J, Burke M. Applications of ground-penetrating radar to glacial and frozen materials. J Environ Eng Geophys, 2007, 12: 69–86
6 Bohren C F, Huffman D R. Absorption and Scattering of Light by Small Particles. New York: Wiley, 1983
7 Hamran S-E, Aarholt E, Hagen J O, et al. Estimation of relative water content in sub-polar glacier using surface-penetration radar. J Glaciol, 1996, 42: 533–537
8 Pettersson R, Jansson P, Blatter H. Spatial variability in water content at the cold-temperate transition surface of the polythermal Storglaciären, Sweden. J Geophys Res, 2004, 109
9 Stolt R H. Migration by Fourier transform. Geophysics, 1978, 43: 23–48
10 Looyenga D E. Dielectric constants of heterogeneous mixtures. Physica, 1965, 31: 401-410
11 Paren J G. Dielectric Properties of Ice. Cambridge, UK: University of Cambridge, 1970
12 Macheret Y Y, Moskalevsky M Y, Vasilenko E V. Velocity of radio waves in glaciers as an indicator of their hydrothermal state, structure and regime. J Glaciol, 1993, 39: 373–384
13 Dix C H. Seismic velocities from surface measurements. Geophysics, 1955, 34: 180–195
14 Redman J D, Davis J L, Galagedara L W, et al. Field studies of GPR air launched surface reflectivity measurements of soil water content. In: Procedings of the Ninth Conf on Ground-Penetrating Radar. 2002. Proc SPIE 4758: 4156–4161
15 Huisman J A, Hubbard S S, Redman J D, et al. Measuring soil water content with ground-penetrating radar: A review. Vadose Zone J, 2003, 2: 476–491
16 Lee J. A frequency-dependent pseudospectral simulation for ground-penetrating radar propagation. Masteral Thesis. Seoul: Seoul National University, 2001
17 Sheriff R E. Encyclopedic dictionary of exploration geophysics. 3rd ed. Society of Exploration Geophysicists, 1991
18 Chanzy A, Tarussov A, Judge A, et al. Soil water content determination using a digital ground-penetrating radar. Soil Sci Soc Am J, 1996, 60: 1318–1326
19 Irvine-Fynn T D L, Moorman B J, Williams J L M, et al. Seasonal changes in ground penetrating radar signature observed at a polythermal glacier, Bylot Island, Canada. Earth Surf Process Landforms, 2006, 31: 892–909
20 Fountain A G, Jacobel R W, Schlichting R, et al. Fractures as the main pathways of water flow in temperate glaciers. Nature, 2005, 433: 618–620
21 Kim K Y, Hong M H, Lee J, et al. Seismic experiments on the Fourcade Glacier in the King George Island. Antarctica. In: EGU. Geophysl Res Abs, 2007, 9: 04755
22 Navarro F J, Macheret Y Y, Benjumea B. Application of radar and seismic methods for the investigation of temperate glaciers. J Appl Geophys, 2005, 57: 193–211
23 Hambrey M J, Müller F. Ice deformation and structures in the white glacier, Axel Heiberg Island. J Glaciol, 1978, 25: 215–228
24 Stuart G, Murray T, Gamble N, et al. Characterization of englacial channels by ground-penetrating radar: An example from austre Brøggerbreen, Svalvard. J Geophys Res, 2003, 108(B11): 2525